www.sciencemag.org/content/355/6331/1312/suppl/DC1

Supplementary Materials for

A conserved NAD^+ binding pocket that regulates protein-protein interactions during aging

Jun Li, Michael S. Bonkowski, Sébastien Moniot, Dapeng Zhang, Basil P. Hubbard, Alvin J. Y. Ling, Luis A. Rajman, Bo Qin, Zhenkun Lou, Vera Gorbunova, L. Aravind, Clemens Steegborn, David A. Sinclair*

*Corresponding author. Email: david_sinclair@hms.harvard.edu

Published 24 March 2017, *Science* **355**, 1312 (2017)
DOI: 10.1126/science.aad8242

This PDF file includes:

Materials and Methods

Chemical reagents

All chemicals were purchased from Sigma Aldrich, with the following exceptions: PJ34 (Orchid Pharmaceuticals), 3-AB (Calbiochem) and EX-527 (Tocris Bioscience). NR and carba-NAD were synthesized and provided by Sirtris, a GSK company.

Constructs/mutagenesis

The constructs used for stable expression of full-length and truncated human Flag-DBC1, have been previously described (*25*). The transient expression plasmids for human pcDNA 3.1 V5/His-DBC1 were constructed by cloning human DBC1 cDNA into pcDNA3.1 vector. Myc-DDK-tagged human PARP1 (Flag-PARP1) was purchased from OriGene (RC207085). Point mutants or deletion mutants for Flag-DBC1, V5/His -DBC1 or Flag-PARP1 were generated using Quickchange II XL Site Directed Mutagenesis kit (Stratagene), and verified by DNA sequencing (Dana-Farber/Harvard Cancer Center DNA Resource Core, Boston, MA). The constructs overexpressing mouse NMNAT1: pEGFP-N1 vector and pEGFP-N2-NMNAT1, were gifts from Dr. Shin-Ichiro Imai, Washington University School of Medicine (*26*). The constructs overexpressing the rat BRCT domain of PARP1 was a gift from Dr. Robert London, National Institute of Environmental Health (27). The construct overexpressing human MACROD1 was purchased from Addgene (#39041). The constructs overexpressing the catalytic domain of human PARP1 was a gift from Dr. Lee Kraus, University of Texas Southwest Medical Center (28). The shRNA constructs for SIRT1 (TRCN0000018979, TRCN0000018983) and DBC1 (TRCN0000053723 and TRCN0000053725) were both in pLKO.1 vector and purchased from Open Biosystems. The control shRNA for both SIRT1 and DBC1 was a TRC lentiviral pLKO.1 vector (# RHS4080). The siRNAs for human DBC1 (sc-72274), human PARP1 (sc-29437) and control siRNA (sc-36869) were from Santa Cruz.

Cell Culture, Transfection and Infection

293T, MCF-7, DBC1 wild-type and knockout MEFs (a gift from Dr. Eduardo N. Chini from Mayo Clinic) were cultured in Dulbecco's modified Eagle's medium (DMEM, Mediatech, Inc., Herndon, VA) supplemented with 10% fetal bovine serum (Gemini Bio-products, Woodland, CA) with the presence of penicillin and streptomycin (Corning, Manassas, VA). Retroviruses expressing wild-type or mutant Flag-DBC1 proteins were produced by transfecting 293T cells with plasmids encoding VSV-G, Gag-Pol, and pMSCVpuro-Flag-DBC1 constructs using Lipofectamine® 2000 according to the manufacturer's instructions. Media was changed the day after transfection, and virus-containing media was harvested between 48 and 72 hours post-transfection and filtered through a 0.45 mm filter (Corning, Manassas, VA). The filtered media was incubated with the target cells in the presence of 5μg/mL polybrene (Sigma) and selection started using puromycin (2 μg/mL) 48 hrs post-infection. Lentivirus for knocking down DBC1 or SIRT1 was produced by transfecting 293T with psPAX2 (Addgene plasmid #12260), pMD2.G (Addgene plasmid # 12259) and shRNA constructs using Lipofectamine® 2000. The virus harvest, infection and selection were same as described for retrovirus production. The transfections of siRNA were performed using Lipofectamine® RNAiMAX, according to the manufacturer's instructions.

The human primary fibroblast cells were cultured in Dulbecco's modified Eagle's medium supplemented with 15% fetal bovine serum in a low oxygen incubator (3% oxygen, 5% CO_2, 37°C).

Immunoprecipitation

Protein extracts from 293T or mouse liver tissues were lysed in ice-cold buffer (150 mM NaCl, 1 mM EDTA, 1 mM EGTA, 1 % Triton X-100, 0.5% NP-40, 10 mM Tris HCl, pH 7.4) supplemented with protease inhibitors cocktail cOmplete tablets (Roche) and phosphatase inhibitor cocktail 2 and 3 (Sigma). Protein concentrations were determined by the Bradford protein assay (Bio-rad). Flag-M2 agarose beads or anti-V5 agarose affinity gel (Sigma) were mixed with the lysate supernatant. Immunoprecipitation was allowed to proceed for 2 hours up to overnight at 4˚C with gentle rotation. After 4 washes with lysis buffer, proteins were either directly boiled in SDS-PAGE sample buffer or eluted from the agarose beads using 3X FLAG peptides (Sigma).

Immunoblotting

Cell lysates or Co-IP samples were run on homemade 10% or 4-20% gradient pre-cast SDS-PAGE gels (Bio-Rad) under reducing conditions, and then transferred to a polyvinylidene difluoride (PVDF) membrane (Millipore). Membranes were blocked with 5% non-fat dry milk in TBS-Tween (10 mM Tris HCl, pH 7.5, 150 mM NaCl, and 0.1% Tween-20). Antibodies were used at the following concentrations: anti-SIRT1 (Santa Cruz, SC-15404) at 1:500, anti-DBC1 (Bethyl Labotatories, A300-434A) at 1:1000, anti-PARP1 (Cell Signaling, #9542L) at 1:1000, anti- γH2AX (Abcam, ab2893) at 1:1000, anti-H2AX (Abcam, ab11175) at 1:1000, anti-NMNAT1 (Abcam, ab45548) at 1:1000, anti-GAPDH (Millipore, MAB374) at 1:3000, anti-V5 (Invitrogen, R960-25) at 1:3000, anti-beta-tubulin (Upstate, 05-661) at 1:1000, anti-α-actin (Millipore, MAB1501R) at 1:2000, anti-Flag (Sigma, F7425) at 1:3000, anti-PARG (Abcam, ab16060) at 1:1000, p53 (Calbiochem, OP43) at 1:1000, RAD51 (Calbiochem, PC130) at 1:1000, p21 (Neomarker-Labvision-Thermal Fisher, RB-032-P1) at 1:1000, SIRT6 (Cell signaling, D8D12) at 1:1000, Streptavidin-HRP at 1:1000 (Trevigen #4800-30-06), anti-PAR (Trevigen, #4335-MC-100; Abcam, ab14459) at 1:1000 and anti-PARP2 (Santa Cruz, SC-393310) at 1:200 overnight at 4ºC. The antibodies ATM, ATR, BRCA1, Chk1, Chk2, DNA-PKs and XRCC1 were all from the Bethyl Laboratories. Phospho-Chk1, phospho-Chk2 and phosphor-p53 antibodies were from a DNA Damage Antibody Sampler Kit (Cell Signaling #9947). Secondary antibodies were horseradish peroxidase-coupled sheep anti-mouse IgG (GE Healthcare, UK), donkey anti-rabbit IgG (GE Healthcare, UK). Amersham TM ECL and Amersham Select ECL western blotting detection systems (GE Healthcare, UK) were used to develop signals. Quantifications of images from western blot films were performed using ImageJ (National Institutes of Health, Bethesda, MD).

PARP1-DBC1 dissociation assays

Equal aliquots of 293T cell lysates with over-expressing Flag-DBC1 were immunoprecipitated using Flag-M2 agarose beads as described above. After four brief washes with lysis buffer, the beads aliquots were incubated with the freshly dissolved

NAD^+ or other chemicals for 1 hr at 4˚C with gentle rotation then centrifuged (5000 rpm, 5 min). After completely removing supernatant, the beads were boiled in SDS loading buffer, analyzed by SDS-PAGE, and probed with antibodies.

NAD^+ Quantification

NAD^+ quantification was conducted with an NAD/NADH Quantification Kit (Biovision, Milpitas, CA) following the manufacturer's instructions and normalized to soluble protein content.

^{32}P-NAD^+ binding assays

Empty vector (6 μg), wild type, $DBC1_{Q391A}$ and $DBC1_{\Delta 354\text{-}396}$ (pcDNA 3.1 vector with V5/his tag) were transfected into 293T cells in 15 cm petri dishes separately, followed by IP using anti-V5 agarose gel as described above. After immunoprecipitation, 1/8 of the purified DBC1 protein bound to beads was boiled in SDS loading buffer and assessed for protein input by dot blotting. The remainder of the protein was incubated with cold NAD^+ (1 μM), 8 μCi ^{32}P NAD^+ (PerkinElmer) in 50 μl incubation buffer (50 mM Tris HCl, 150 mM NaCl and 10mM DTT, pH7.4) for 2 hrs at 4˚C with gentle rotation. Beads were then washed in 1 ml of the same incubation buffer 3 times, centrifuged, and eluted in 25 μl of incubation buffer with 10 μg/ml V5 peptides on ice for 30 min with occasional shaking. Each elutant (5 μl) was spotted on filter paper and assessed by autoradiography.

Biotin-NAD^+ binding assays

Lysates of 293T cells expressing Flag-DBC1 or V5/his-DBC1 were prepared as described above and bound to an anti-Flag high sensitivity M2 coated 96-well plate (Sigma) or His-select® high sensitivity nickel coated 96-well plate (Sigma) by incubating for 3-4 hrs at 4˚C, then washed three times with lysis buffer. Biotin-NAD^+ (Trevigen), or specified molecules were incubated in the plates overnight at 4˚C. After washing twice with PBS (pH 7.4) and twice with PBS-T (0.1% Triton X-100), streptavidin-HRP (Trevigen, 1:500) in PBS-T was added to each well and incubated for 1 hr at room temperature. After washing twice with PBS (pH 7.4) and twice with PBS-T, 100 μl of PeroxyGlow ™ A and B chemiluminescent substrates (Trevigen) mixture (1:1) was added into each well for 1 min followed by immediate quantification of chemiluminescence on a EnSpire 2300 Multi-label reader (Perkin Elmer). Binding curves were calculated using the "one site, specific binding" formula of GraphPad.

Cell survival

The CellTiter 96® Aqueous One Solution Cell Proliferation Assay (MTS) kit from Promega was used to measure cell survival after treating cells with paraquat for 24 hrs, according to manufacturer's instructions. The absorbance was measured using an EnSpire 2300 Multi-label reader (Perkin Elmer).

PARP1 activity assay

PARP1 was immunoprecipitated from cell or tissue extracts and activity was determined by a Universal Chemiluminescent PARP Assay Kit (Trevigen, # 4676-096-K)

that is based on HRP-streptavidin-mediated detection of biotin-labelled PAR. Luminescence was measured on an EnSpire 2300 Multi-label reader (Perkin Elmer).

Comet assay

The CometAssay® kit (Trevigen) was used to detect DNA fragmentation in DBC1 knockdown 293T cells. After treatment with paraquat for 24 hrs, the cells were gently harvested and embedded in an agarose layer on microscope slides provided by the kit. Cells were lysed and DNA was electrophoresed for 30 min at 1 Volt/cm in alkaline conditions. Tails were visualized at a magnification of 200× using a Nikon Eclipse Ti microscope. The comet analysis open software casp_1.2.3b1 was used (casplab.com) to analyze randomly chosen nuclei (n>50) per group.

8-OHdG DNA damage quantification

The OxiSelect™ oxidative DNA damage Elisa kit (Cell Biolabs) was used to detect 8-OHdG in mice livers after irradiation. Genomic DNA was extracted from liver using a DNeasy blood and tissue kit (Qiagen).

Gene Expression Analysis

MCF-7 Cells were trypsinized and washed in PBS before RNA was extracted using an RNeasy Mini Kit (Qiagen) and quantified using a NanoDrop 1000 spectrophotometer (Thermo Scientific). The cDNA synthesis was performed with iScript ™ cDNA Synthesis Kit (Bio-Rad). Quantitative RT-PCR reactions were performed using LightCycler® 480 SYBR Green Master (Roche) on a LightCycler® 96 Real-Time PCR System (Roche). Calculations were performed using GeneEx qPCR data analysis software from Bio-Rad. Gene expression was normalized to housekeeping gene HPRT. Primers used for qPCR: HPRT: TGCTGAGGATTTGGAAAGGG and ACAGAGGGCTACAATGTGATG; ABHD2: CACCTCTCTGAGCCTGTTCC and CGCAGATGTTCAGCAATGTT; TMSNB: TCCCAACAGCAGATTTCGAC and GCCAGGGAACATAGGTGAGA; PEG10: CAAGCCACCACCAGGTAGAT and GAGGCACAGGTTCAGCTTTC; NELL2: TGAAGGGAACCACCTACC and ATTTGCCATCCACATACG.

Mouse handling and treatment

C57BL/6J mice were obtained from the National Institutes of Aging (Bethesda, MD) or The Jackson Laboratory (Bar Harbor, ME). Treatment with PBS, NMN (i.p. 500 mg/kg/day) or Olaparib (i.p. 100mg/kg/day) has been described previously (*29*). Olaparib (Selleckchem) was first dissolved in DMSO as a stock solution and diluted to final concentrations with the vehicle 10% w/v 2-hydroxypropyl-b-cyclodextrin in PBS prior to injection (Sigma, H107-5G). Mice were allowed to acclimatize to the facility for at least three weeks and all animal procedures were in accordance with the animal care and use policies of the IACUC committee at Harvard Medical School.

Protein sequence analysis, structural modeling and docking

Iterative profile searches with the PSI-BLAST program (*30*) were used to retrieve homologous sequences from the protein non-redundant (NR) database at National Center for Biotechnology Information (NCBI). Multiple sequence alignments were built using

the Kalign (*31*) and Promals (*32*) programs, followed by careful manual adjustments based on profile–profile alignment derived using the HHpred program (*33*), secondary structure prediction using the Jpred program (*34*) and using structural alignments. The Modeller9v11 program (*35*) was utilized for homology modeling the 3-dimentional structure of DBC1-NHD by using multiple PDB templates including *Shewanella oneidensis* NrtR (3gz5), *Aquifex aeolicus* Nudix hydrolase (2yyh), *Caenorhabditis elegans* AP4A hydrolase (1ktg), *Mycobacterium tuberculosis* ADPr pyrophosphatase (1mk1), and *Escherichia coli* GDP mannose hydrolase (1rya). In these low-sequence-identity cases, sequence alignment is the most important factor affecting the quality of the model (*36*). Alignments were therefore carefully built and cross-validated on the basis of information from HHpred and DaliLite programs, then edited manually using secondary structure information. The model was further refined using KoBaMIN (*37*). Autodock Vina was implemented in PyRx (http://pyrx.sorceforge.net) for molecular docking analysis, followed by a docked configuration that was based on the known nucleotide binding modes of Nudix enzyme-substrate complexes.

Immunohistochemistry and Immunofluorescence

The fresh frozen tissues were sectioned on a Minotome Cryostat (International Equipment Co. USA), fixed in pre-cooled acetone (-20°C) for 10 min, rinsed in ice-cold PBS buffer (pH 7.4) 3 times for 5 min, then incubated in H_2O_2 solution in PBS (0.3% v/v) at room temperature for 10 min to block endogenous peroxidase activity, followed by rinsing in PBS 3 times for 5 min. After incubating with blocking buffer (1% fetal bovine serum in PBS with 0.05% Tween 20) in a humidified chamber at room temperature for 1 hr, the slides were incubated with γ-H2AX antibody (1:200 dilution, Cell signaling, #2577) in blocking buffer for 1 hr at room temperature, rinsed with PBS 3 times for 5 min. Anti-rabbit-Horseradish Peroxidase (GE Healthcare, #NA934) was applied as secondary antibody (1:500 diluted in blocking buffer) at room temperature for 1 hr in a humidified chamber. After rinsing with PBS for 3 times for 5 min, freshly made DAB substrate was applied (Thermo Scientific, #34002, USA) for 5 min, followed by counterstaining using Hematoxylin (Mayer's Hematoxylin, Sigma #26043-05) for 2 min and then rinsing in tap water for 15 min before mounting. For immunofluorescence, nuclei were detected by DAPI (Vectashield from Vector Lab, #H-1200) and the γ-H2AX antibody (Cell signaling, #2577) was applied at a 1:200 dilution, then detected using an Alexa Flour ® 488 conjugated goat anti-rabbit secondary antibody (Life technology, #A-11034, 1:500 dilution).

Blue native PAGE

The human PARP1-ΔCAT (residue 1 to 654) and human DBC1-NHD (residue 239 to 553) sequences were cloned into a modified pET19 vector and expressed as fusion proteins containing a N-terminal His_{x6}-SUMO tag in *E. coli* Codon+ using an auto-induction method overnight at 20°C in TB medium supplemented with lactose (0.2% v/v). Both proteins were purified by affinity chromatography (His-Trap column, GE Healthcare) and size-exclusion chromatography (Superdex 200, GE Healthcare). For DBC1, the N-terminal tag was digested with SUMO protease at a protein/protein ratio of 1/100 (w/w) overnight at 4°C and a second affinity chromatography was performed to separate the SUMO tag and protease from the target protein. Purified PARP1-ΔCAT and

DBC1-NHD proteins were incubated for 30 min on ice prior to addition of glycerol (20% v/v final concentration) and loaded on a two-layer blue native page (5% and 12.5% acrylamide for the stacking and resolving layers, respectively). The blue native PAGE was then run at 4°C for 2-3 hours at 200V. Marker bands at 240, 67 and 45 kDa corresponding to catalase, bovine serum albumin, and albumin from chicken egg white, respectively, were used to assess molecular weights.

DNA repair reporter assays and FACS analysis

In vivo DNA repair efficiency was measured as described (*38*). Reporter plasmids for measuring NHEJ or HR repair efficiency were linearized by HindIII or I-SceI (NEB) and purified using QIAquick gel extraction kit (Qiagen). Linearized reporter plasmids (0.5 μg) were co-transfected with pDsRed-express-DR (1.5 μg) using Lipofectamin 2000. Cells were treated with paraquat or 3-AB in 24 hrs post-transfection.

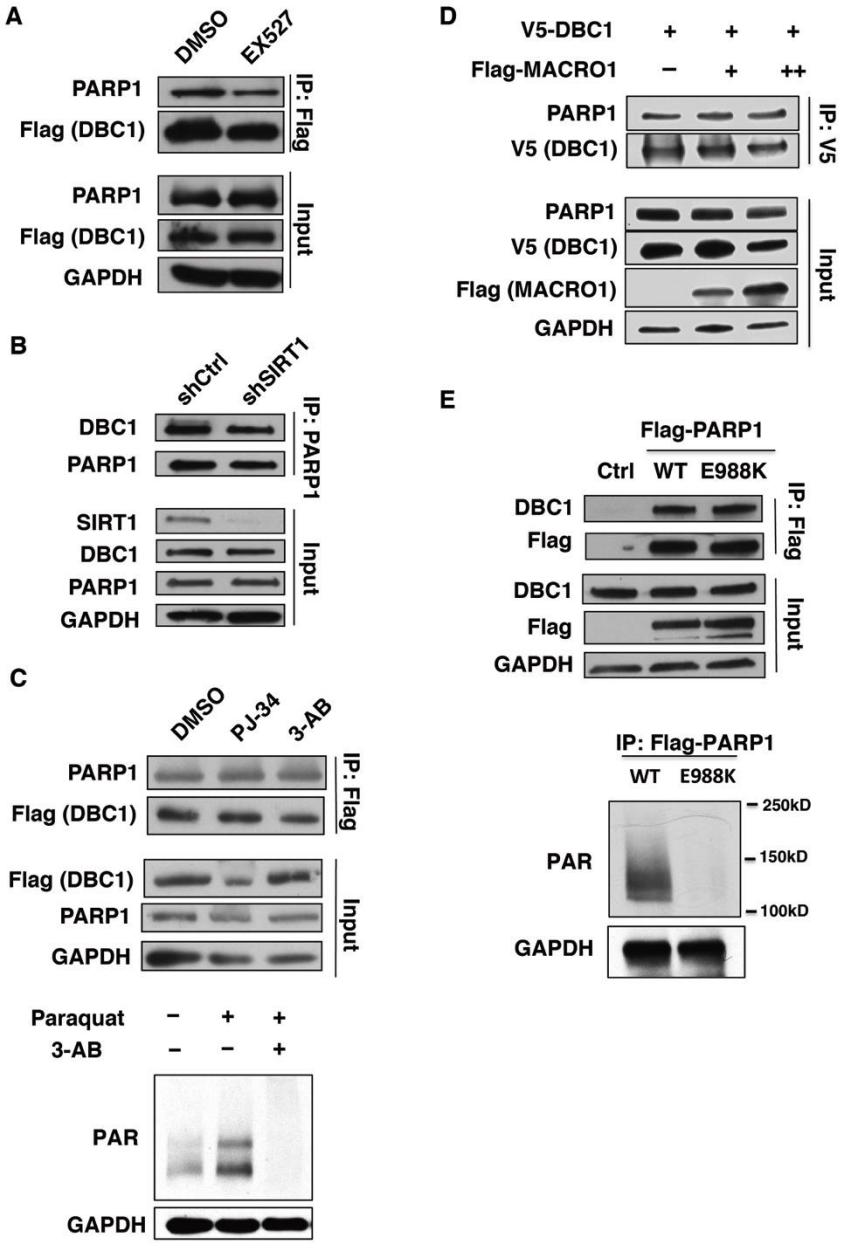

Fig. S1. PARP1-DBC1 complex formation is independent of SIRT1 or PARP1 activity.

(**A**) PARP1-DBC1 interaction in the presence the SIRT1 inhibitor EX527 (20 μM, 24 hrs). (**B**) Effect of SIRT1 knockdown on the PARP1-DBC1 complex. (**C**) The PARP1-DBC1 interaction in the presence of the PARP1 inhibitors PJ-34 (10 μM) or 3-AB (2 mM) for 24 hrs, bottom panel showing inhibitory effect of 3-AB (2 mM) on PAR induced by paraquat (0.5mM). (**D**) Effect of overexpressing MACROD1 on the PARP1-DBC1 complex. DNA transfections: + = 1 μg; ++ = 2 μg. (**E**) Interaction of catalytically inactive PARP1-E988K with DBC1, E988K lacks PAR modification ability, as tested in the bottom panel. All experiments were performed in 293T cells.

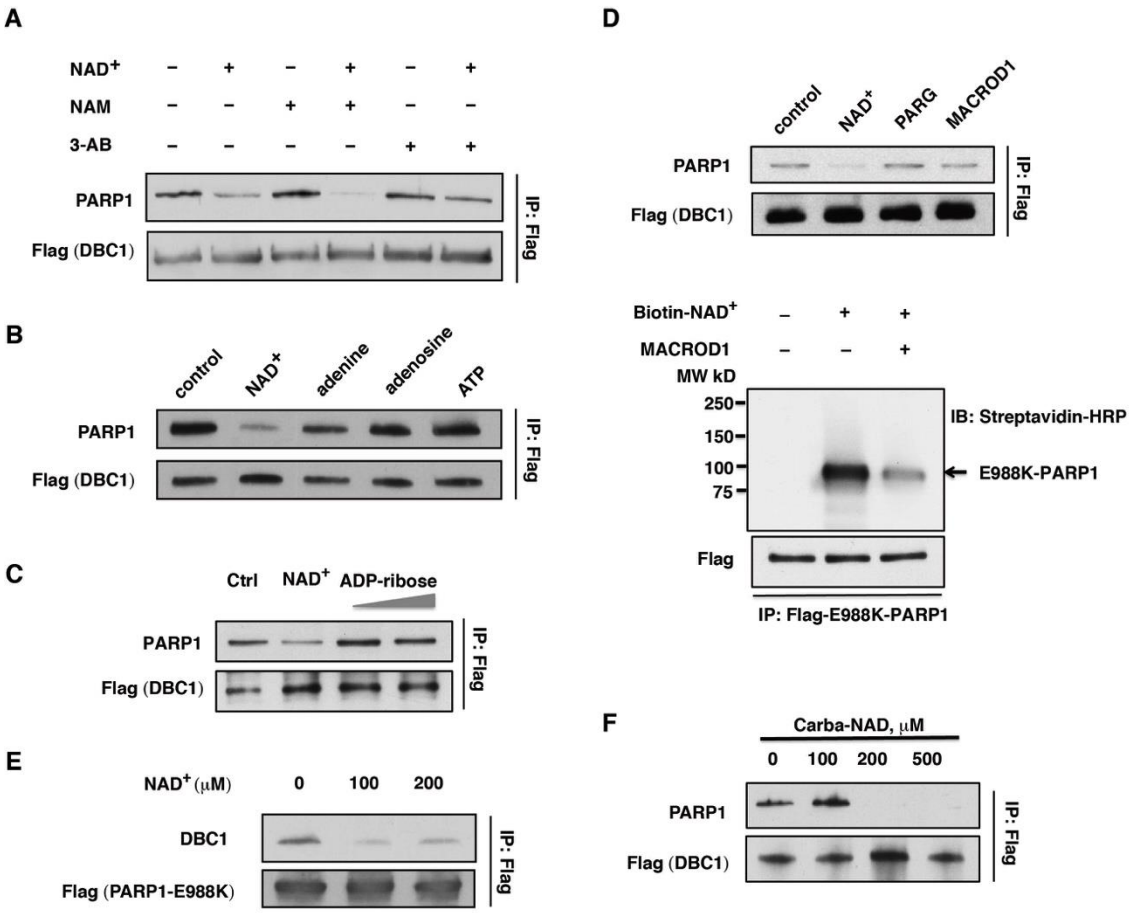

Fig. S2 Effect of NAD$^+$ on the PARP1-DBC1 complex.
(**A**) to (**C**) The PARP1-DBC1 interaction in the presence of molecules structurally related to NAD$^+$: nicotinamide (NAM, 500 μM) and its analogue 3-AB (2 mM), adenine (200 μM), adenosine (200 μM), adenosine triphosphate (ATP, 200 μM), or ADP-ribose (low = 200 μM; high = 500 μM). Flag-DBC1 immunoprecipitates bound to M2 beads were incubated with the above molecules for 1 hr, followed by assessment of PARP1 binding by western blotting. (**D**) Effect of PARG (2 ng) or MACROD1 (1 μg) on the PARP1-DBC1 complex. The activity of MACROD1 purified from bacteria was tested in the bottom panel: E988K-PARP1 was mono-ADPribosylated using biotin-NAD$^+$ as described *(39)*, then de-ADPribosylated by incubating with 1 ug MACROD1 for 30 min as described *(40)*. (**E**) Effect of NAD$^+$ on the interaction between catalytically inactive PARP1-E988K and DBC1. (**F**) Effect of carba-nicotinamide adenine dinucleotide (carba-NAD), a non-hydrolysable NAD$^+$ analogue, on the PARP1-DBC1 complex.

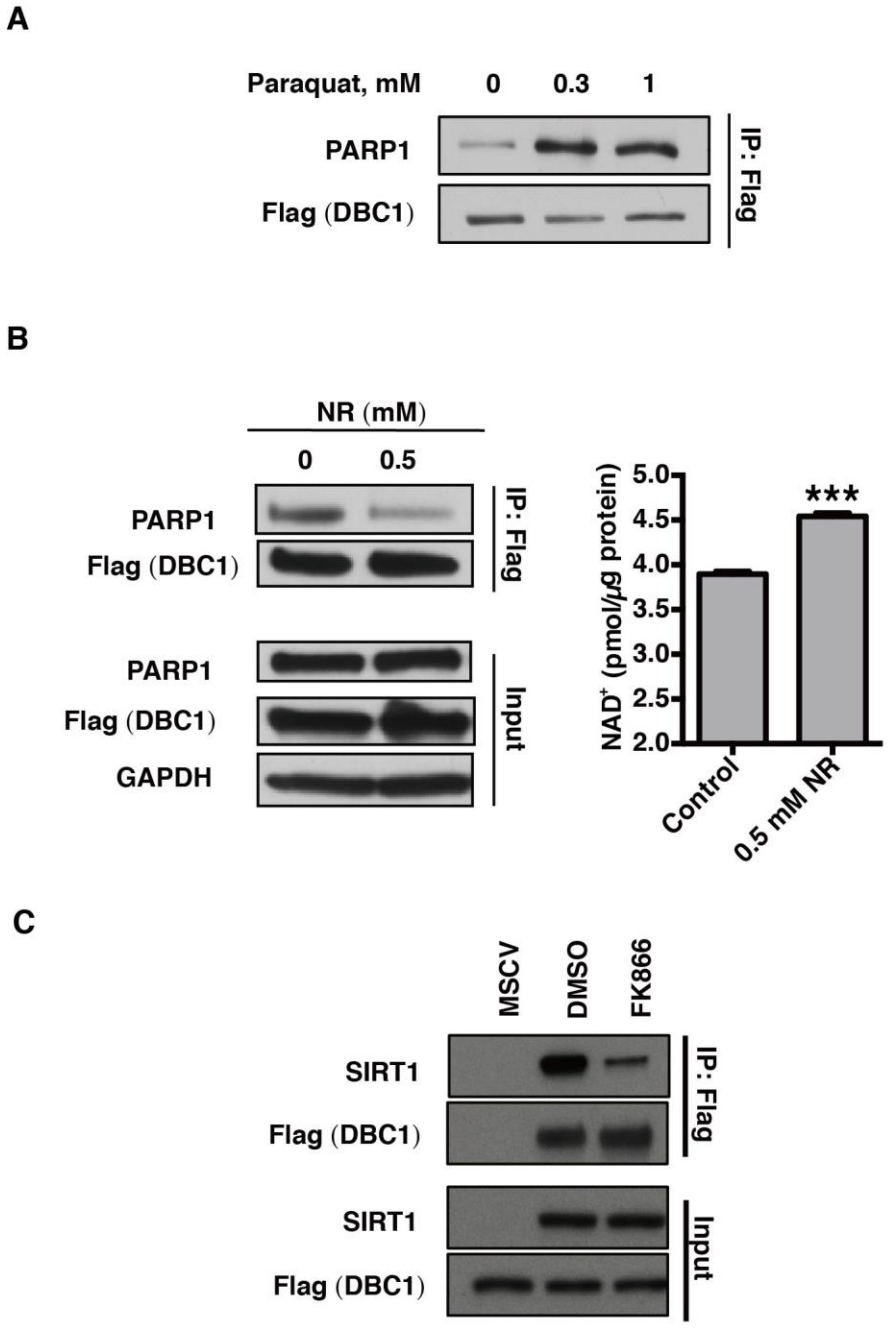

Fig. S3. Effects of NAD^+ levels and DNA damage on the interactions of DBC1 with PARP1.

(A) Effect of paraquat treatment (24 hrs) on the PARP1-DBC1 complex. **(B)** Treatment of 293T cells with nicotinamide riboside (NR) raises cellular NAD^+ levels and dissociates PARP1-DBC1 complex (mean ± SEM, unpaired two-tailed t-test, ***$p<0.001$). **(C)** Effect of the NAMPT inhibitor FK866 (5 nM, 24 hrs) on the SIRT1-DBC1 interaction.

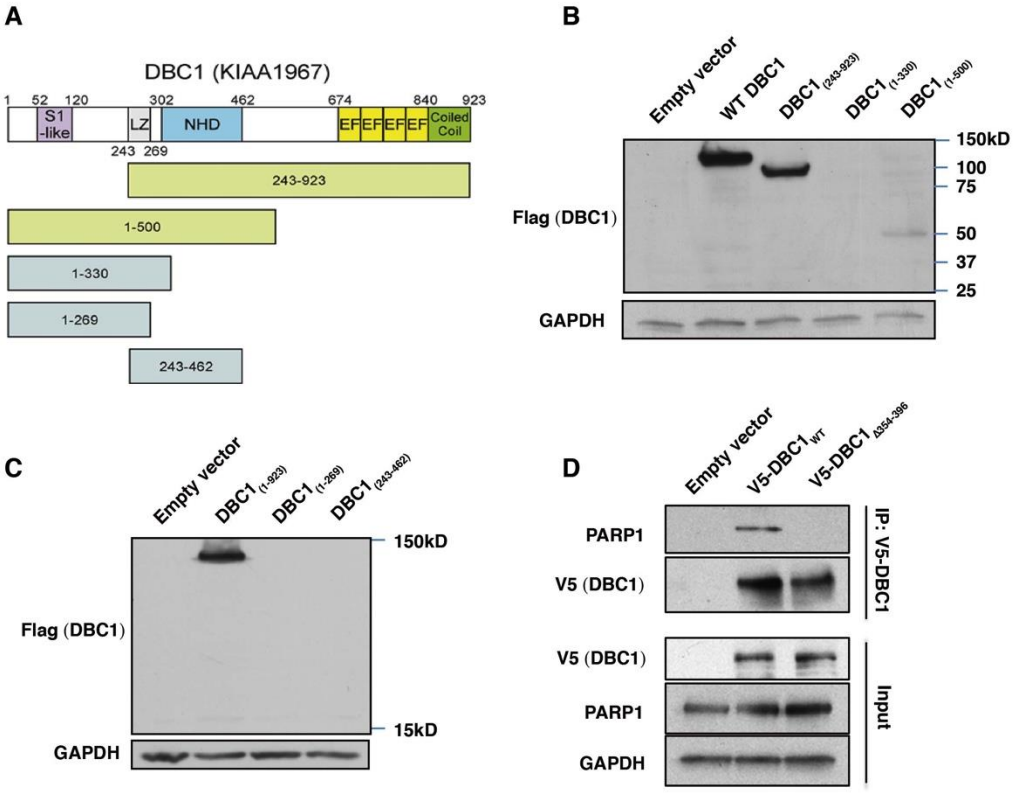

Fig. S4. The PARP1-DBC1 interaction requires the NHD.
(**A**) The DBC1 deletion mutants. Yellow-colored mutants were expressed in 293T cells. Blue-colored mutants could not be expressed. (**B** and **C**) Expression of $DBC1_{(243-923)}$, $DBC1_{(1-500)}$, $DBC1_{(1-330)}$, $DBC1_{(1-269)}$ and $DBC1_{(243-462)}$ in 293T cells. (**D**) Interaction between PARP1 and $DBC1_{(\Delta 354-396)}$, a form of DBC1 lacking partially the NHD.

A

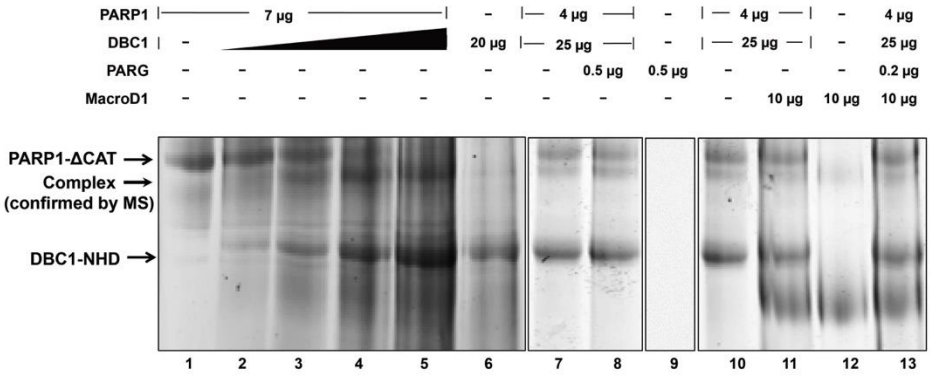

B

Lane	Protein	Number of Spectra	Number of unique peptides	Coverage (%)
5	PARP1	79	44	46.2
	DBC1	28	15	48.7
11	PARP1	52	34	40.0
	DBC1	19	14	35.0
	MACROD1	26	16	38.8
12	MACROD1	26	14	24.9

Fig. S5. Direct binding of DBC1 to PARP1.
(A) Binding of recombinant human PARP1-ΔCAT (residues 1 to 654) to human DBC1-NHD (residue 239 to 553) on blue native poly acrylamide gel electrophoresis in the presence or absence of PARG or MACROD1. **(B)** Mass spectrometry of bands excised from the gel at the size of the DBC1-PARP1 complex to detect proteins present within the indicated region of panel A, lanes 5, 11, and 12.

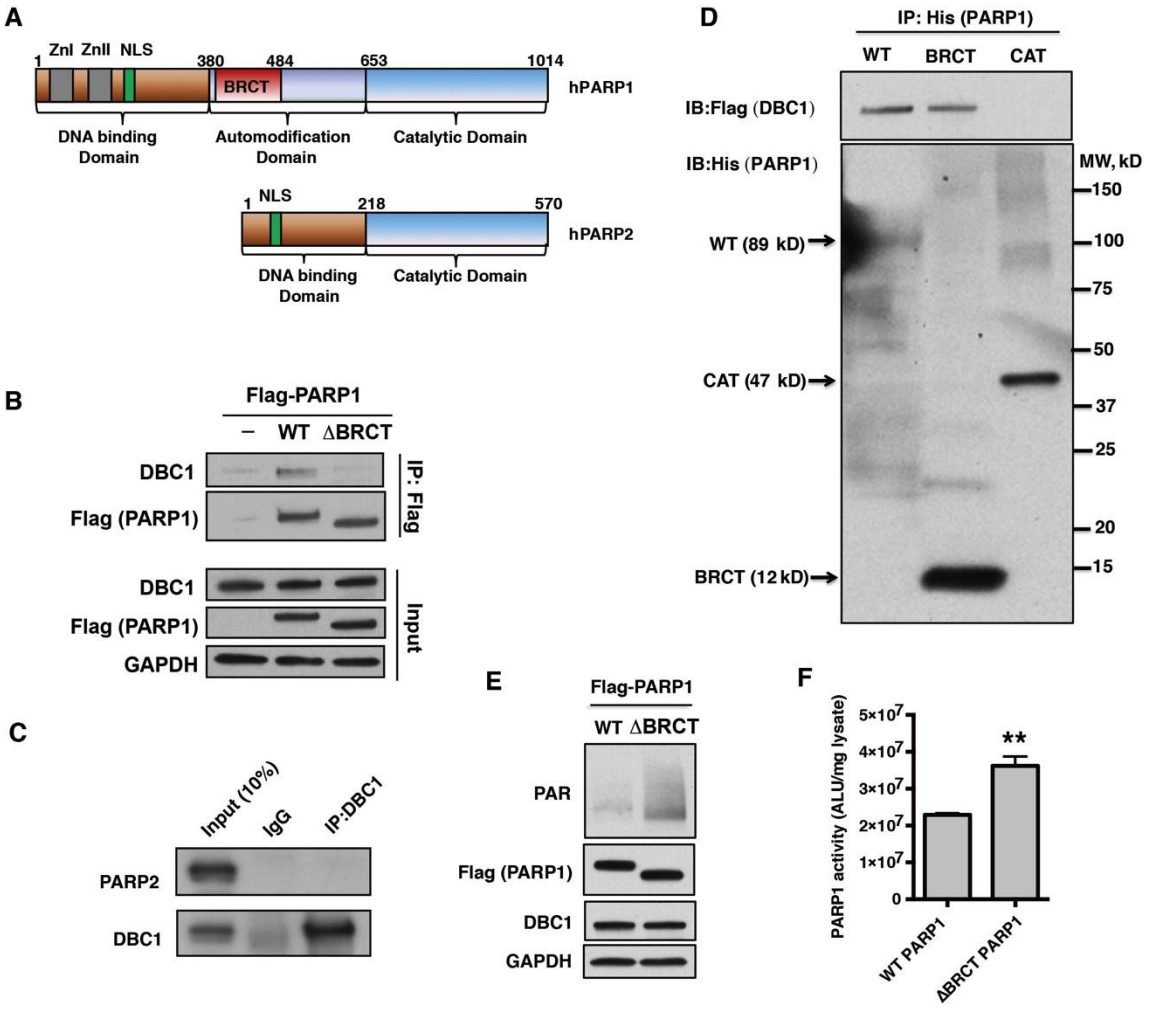

Fig. S6. The PARP1-DBC1 interaction requires the BRCT domain of PARP1.
(**A**) The human PARP1 and PARP2 structures. Zinc finger regions (ZnI and ZnII) and nuclear localization sequence (NLS) are shown. (**B**) Effect of deleting the BRCT domain on PARP1-DBC1 complex formation. (**C**) Lack of an endogenous interaction between PARP2 and DBC1. (**D**) DBC1 interacts with the PARP1-BRCT domain but not PARP1-CAT. Purified His-tagged recombinant proteins were incubated with Flag-DBC1 cell lysate (0.5 mg) overnight and immunoprecipitated using nickel resin and DBC1 was detected by western blotting. Effect of deleting the BRCT domain on (**E**) poly(ADP) ribose (PAR) levels and (**F**) the activity of PARP1 immunoprecipitated from 293T cells, mean ± SEM, unpaired two-tailed t-test, **p<0.01.

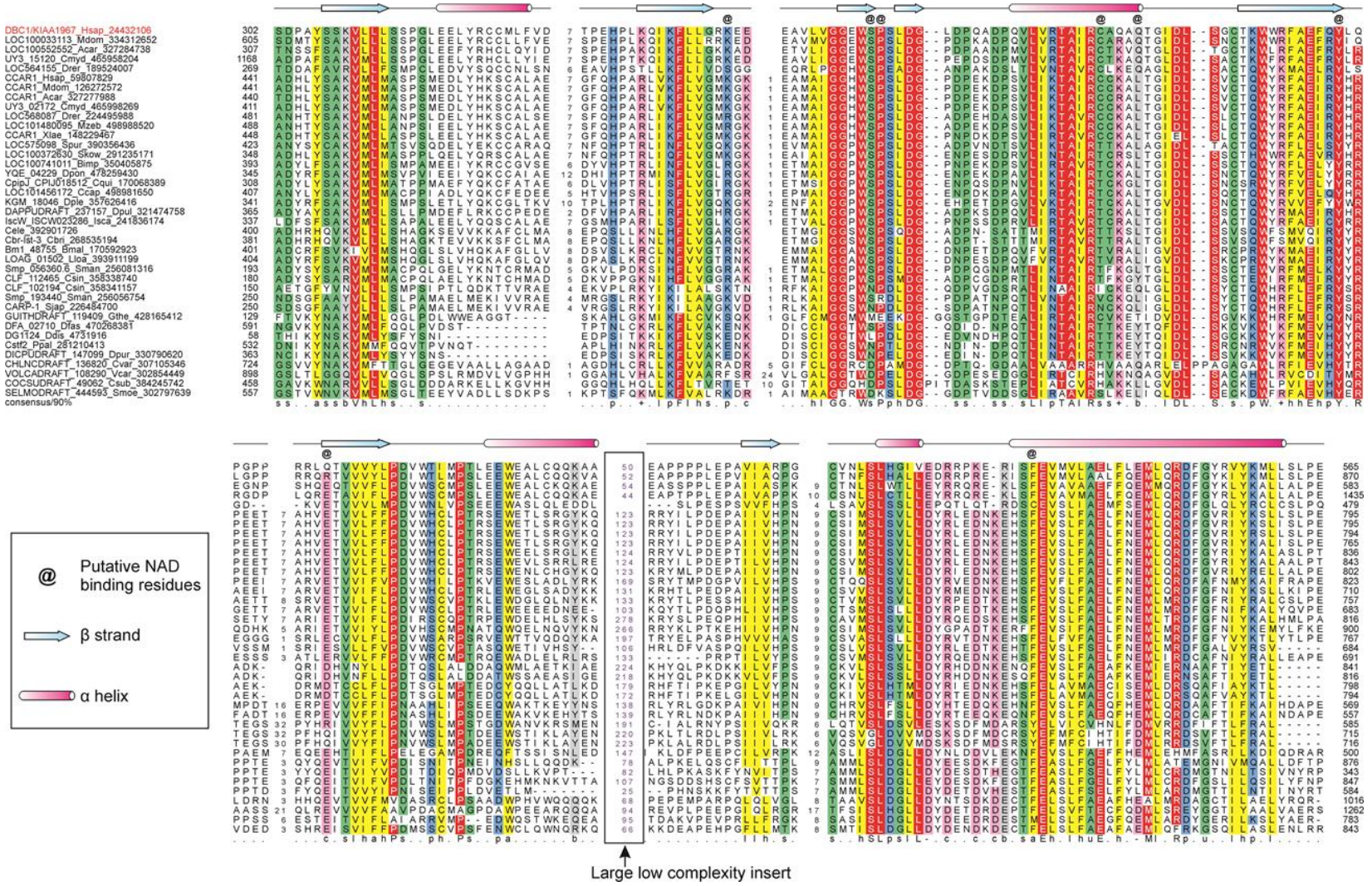

Fig. S7. Multiple Alignments of Nudix domains from various species.
Putative ligand binding residues are indicated by @.

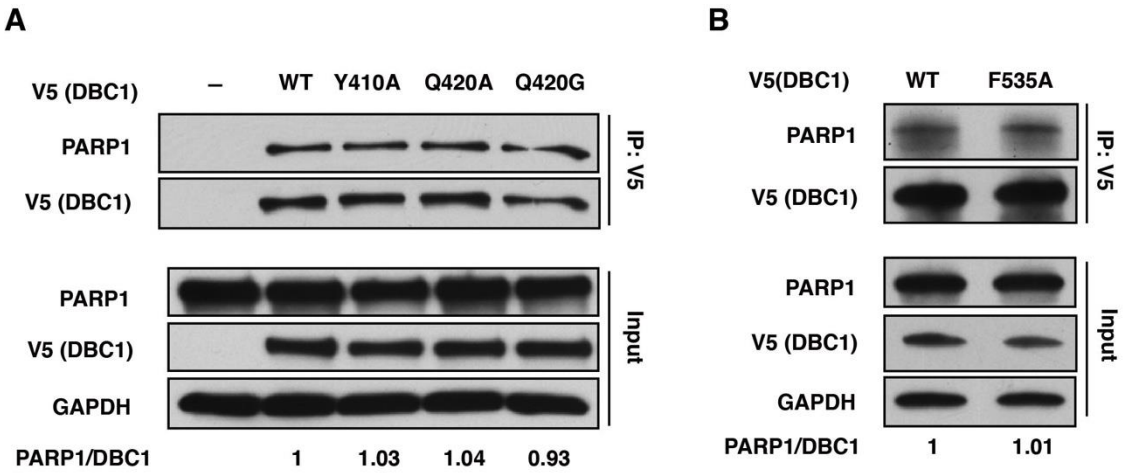

Fig. S8. Representative interactions of DBC1-NHD mutants with PARP1 (continued after Fig. 2B).
The effects of mutating Y410 or Q420 (**A**), or F535 (**B**) on the PARP1-DBC1 interaction. DBC1 was immunoprecipitated using an anti-V5 agarose beads and probed by western blotting for PARP1. Ratio listed below images was determined from band intensities quantified using Image J.

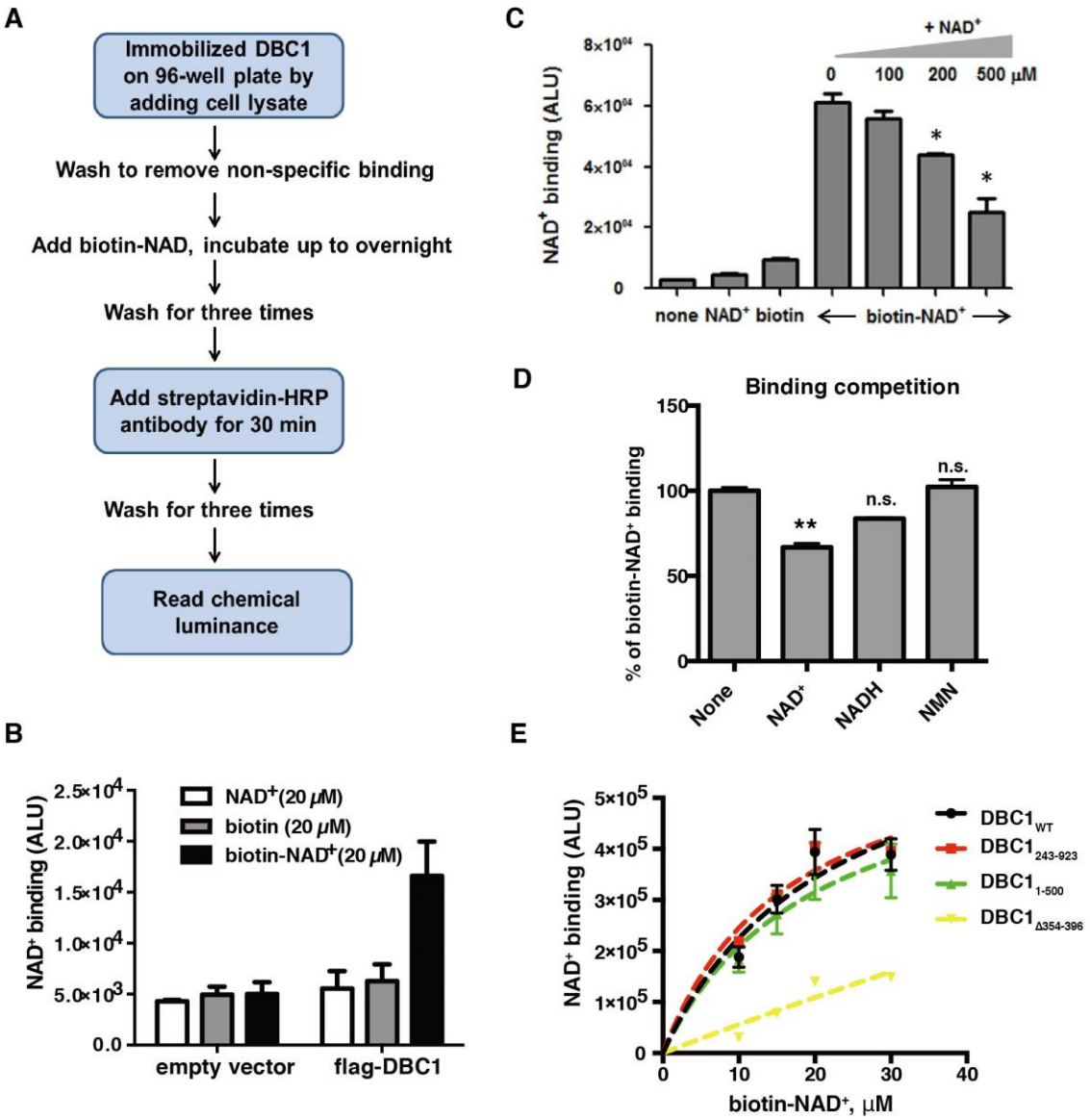

Fig. S9. DBC1 specifically binds to NAD$^+$, which requires its NHD domain.
(**A**) The biotin-NAD$^+$ binding assay. (**B**) Binding of NAD$^+$ to DBC1. Each well was loaded with 0.2 mg of a cell lysate from 293T cells stably transfected with empty vector or Flag-DBC1. (**C**) Competition of biotin-NAD$^+$ with unlabeled NAD$^+$. Flag-DBC1 from cell lysates (0.5 mg) was immobilized in each well and biotin-NAD$^+$ (20 μM) was competed off with unlabeled NAD$^+$ (0-500 μM). (**D**) Effects of NAD$^+$, NADH and NMN on binding of biotin-NAD$^+$ to DBC1. Unlabeled NAD$^+$, NADH or NMN (200 μM) competed against biotin-NAD$^+$ (20 μM). (**E**) Binding curves of $DBC1_{WT}$, $DBC1_{243-923}$, $DBC1_{1-500}$, and $DBC1_{\Delta354-396}$. Kd constants were 22.2, 16.9, 20.6 and 378.7 respectively, determined by GraphPad using one site, specific binding formula. Errors are SEM, one-way *ANOVA* with Sidak's post-hoc correction, *p<0.05, **p<0.01, n.s., not significant.

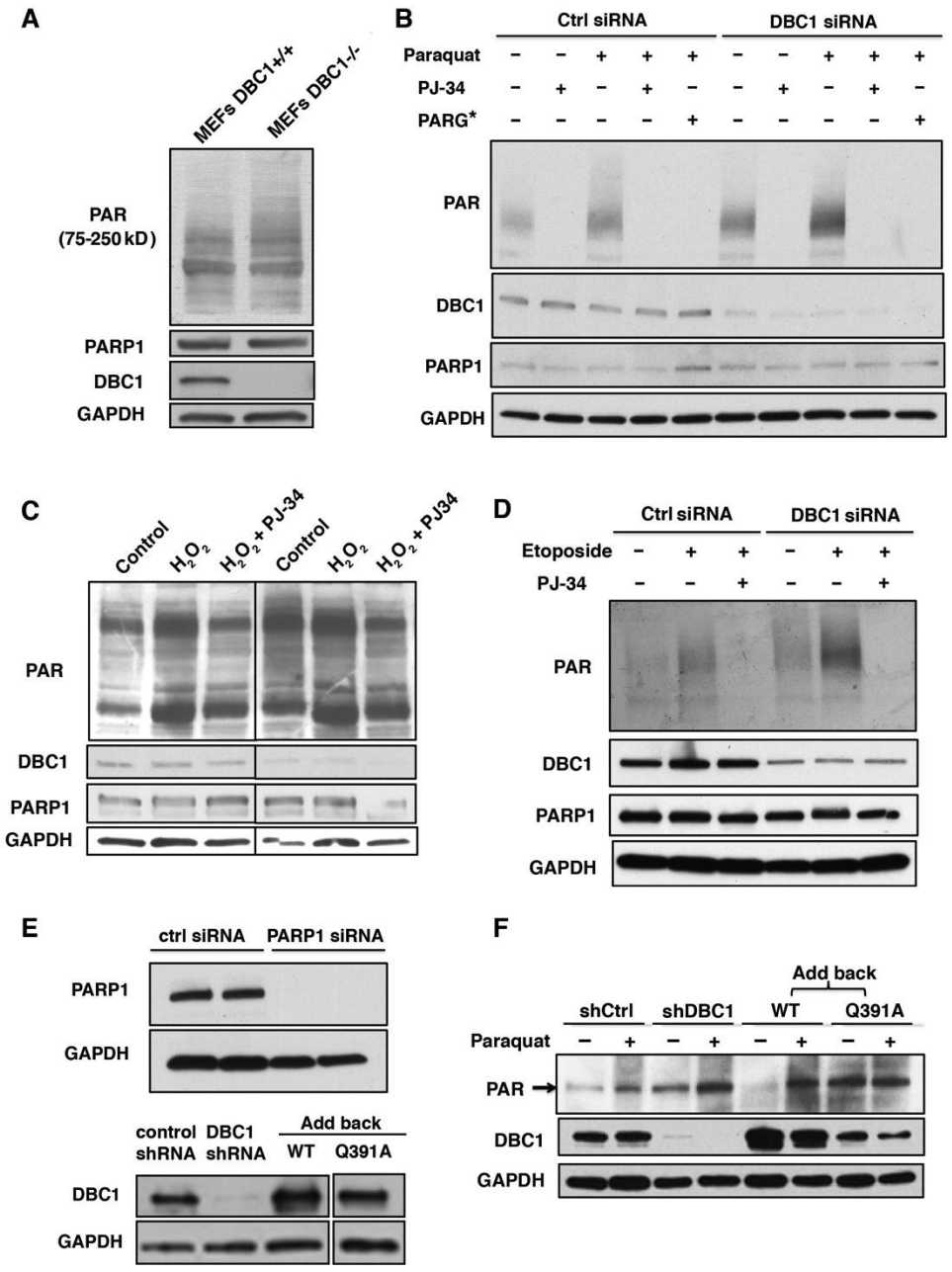

Fig. S10. DBC1 inhibits PARP1 activity in the presence and absence of genotoxic stresses.

(**A**) PAR levels in DBC1 knockout MEFs were determined by western blotting. (**B to D**) Effect of DBC1 knockdown in 293T cells on PAR levels under normal conditions and after treatment with (B) paraquat (0.5 mM, 24 hrs), (C) H_2O_2 (0.2 mM, 30 min) or (D) etoposide (25 μM, 24 hrs). PARG (2 ng) was added into cell lysates to digest PAR for 30 min (*****). (**E**) Assessment of DBC1 protein levels in MCF-7 cells knocked down for DBC1 and reconstituted with mutants from Fig. 3C. (**F**) Effect of re-introducing wild-type DBC1 and DBC1-Q391A on PAR levels.

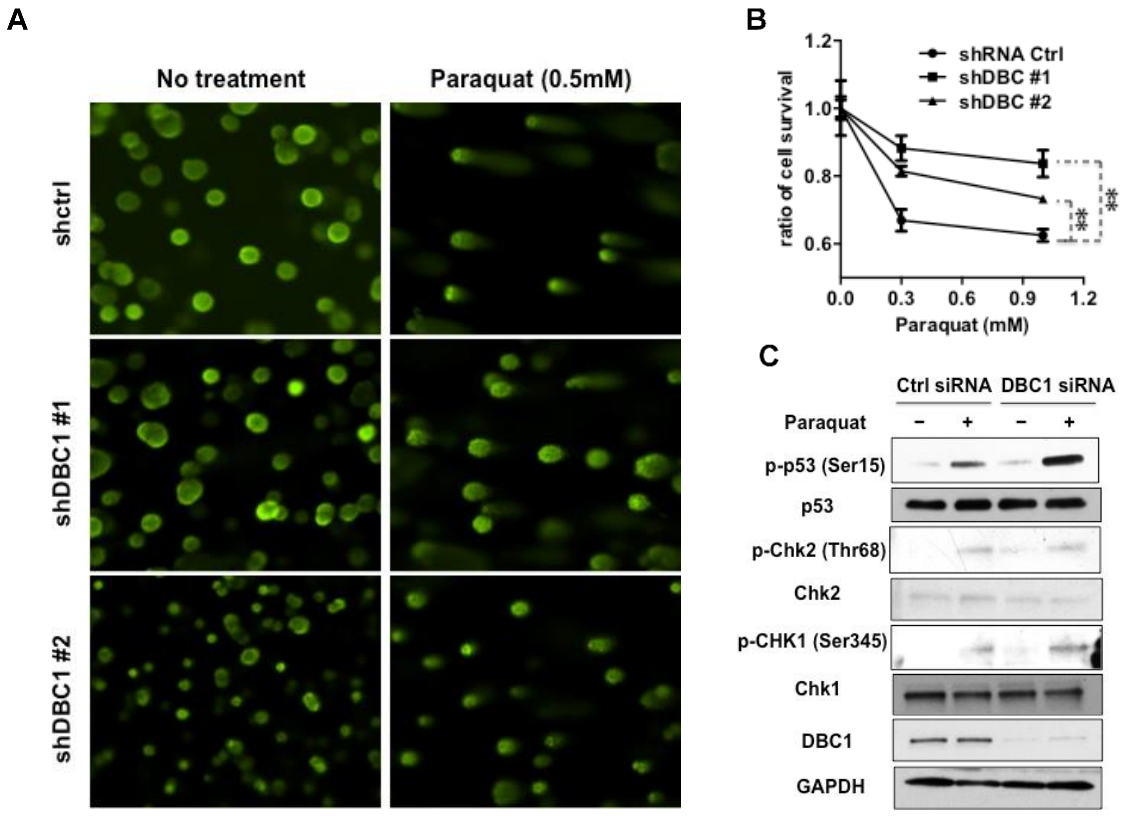

Fig. S11. DBC1 knockdown protects cells from DNA damage by activating DNA repair.

(**A**) Representative images of the comet assay performed on DBC1 knockdown 293T cells after paraquat treatment (0.5 mM, 24 hrs). Images are at 200X magnification. (**B**) Effect of DBC1 knockdown on survival after paraquat treatment (24 hrs), mean ± SEM, unpaired two-tailed t-test, **p<0.01. (**C**) Effect of knocking down DBC1 on DNA damage response pathways in 293T cells treated with paraquat (0.5 mM, 24 hrs). Western blotting was used to detect phosphor-Chk2 (Thr68), Chk2, phosphor-Chk1 (Ser345), Chk1, phosphor-p53 (Ser15), p53, DBC1. GAPDH served as a loading control.

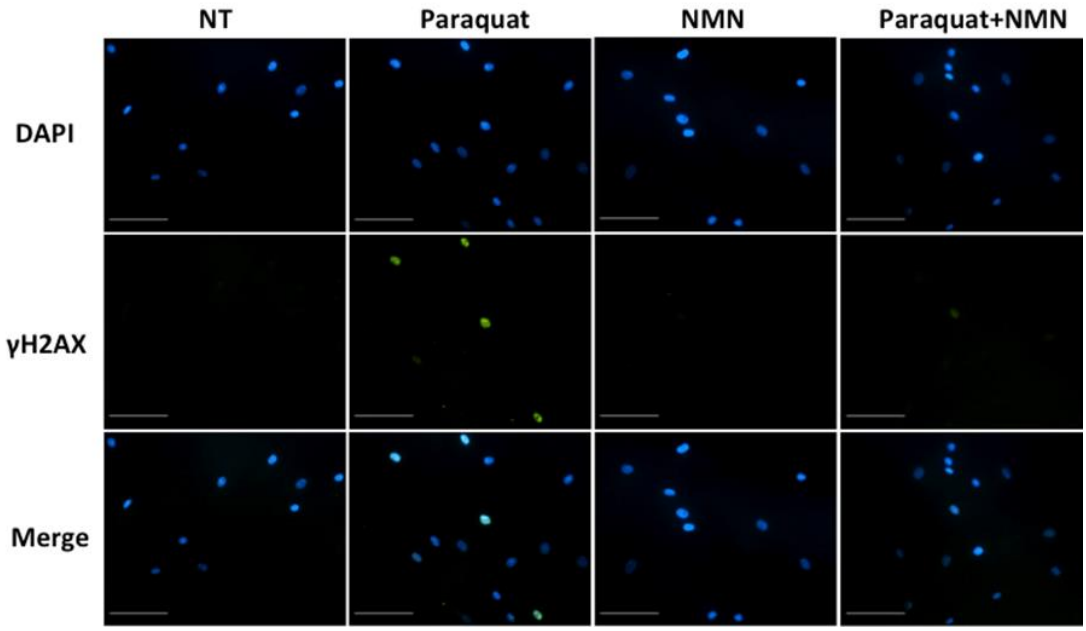

Fig. S12. NMN reduces DNA damage in primary human fibroblasts
Representative images of the immunofluorescence experiment in Figure 3G. Scale = 50 μM. Two fibroblasts cell lines from 94- and 57-year old males (Coriell Institute, #AG08433 and #AG13145) were treated with NMN (500 μM), paraquat (300 μM), or both for 24 hrs at passages 12-13 and immunostained for γH2AX.

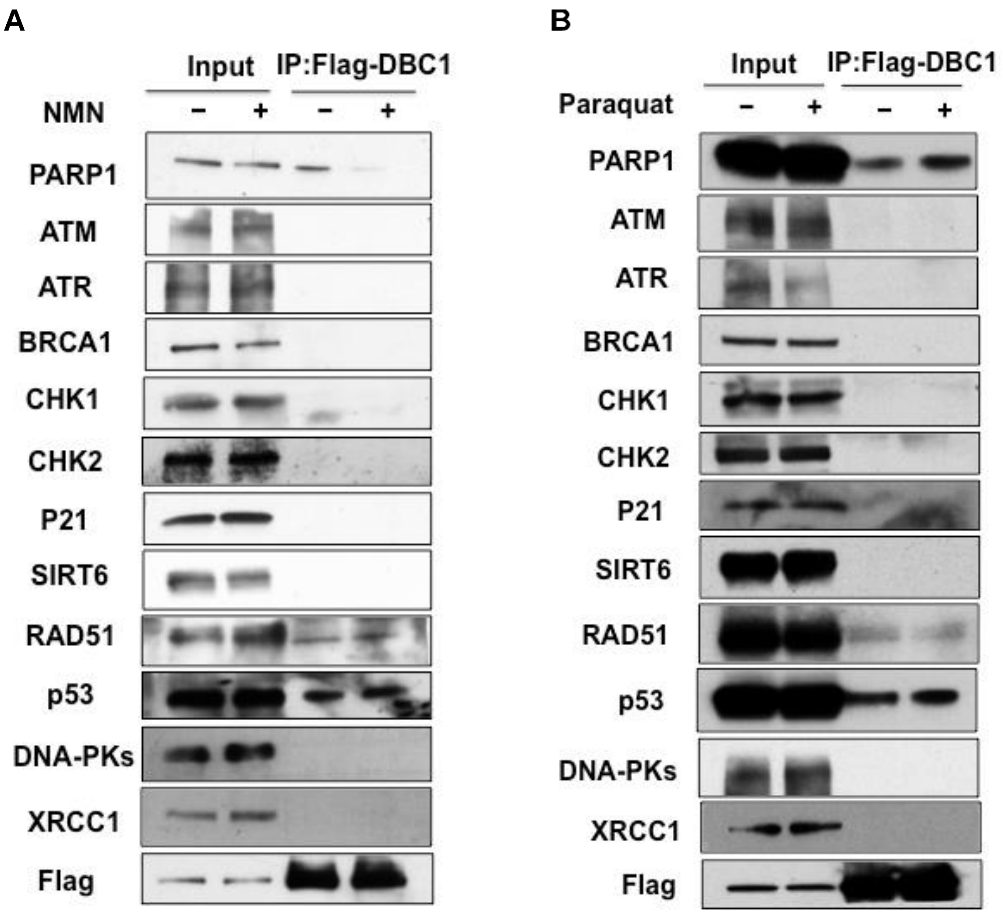

Fig. S13. DNA damage and NAD^+ levels do not change the interaction of major DNA repair proteins with the PARP1-DBC1 complex.
293T cells overexpressing Flag-DBC1 were treated with **(A)** NMN (0.5 mM) or **(B)** paraquat (0.5 mM) for 24 hrs. Flag-DBC1 was immunoprecipitated and DNA repair proteins were assessed by western blotting as indicated. Both p53 and RAD51 were pulled down with Flag-DBC1 and the interaction did not change with treatment of NMN or paraquat.

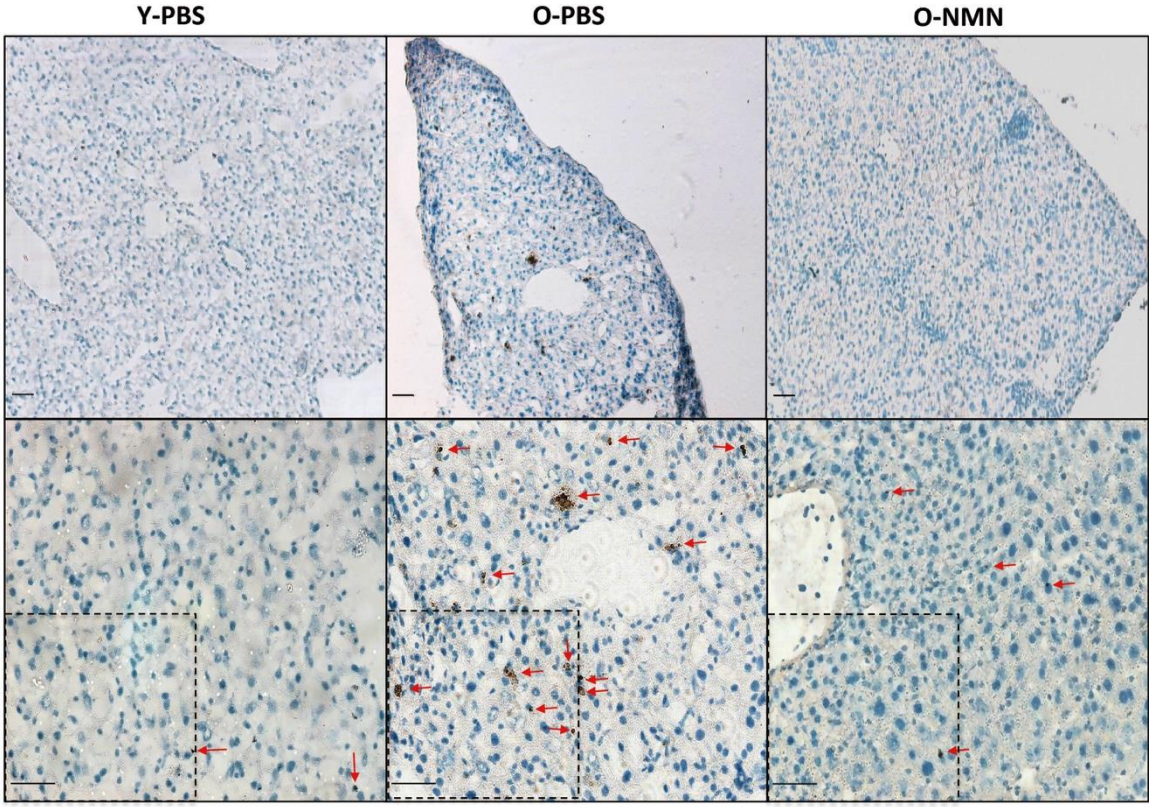

Fig. S14. NMN treatment decreases DNA damage in livers of old mice.
Spontaneous DNA damage in the livers of young and old mice treated with PBS or NMN as in Figure 4C. γH2AX-positive cells were detected by DAB-immunohistochemistry. Positive cells indicated by red arrows. Young (Y) = 6 months, n = 4; old (O) = 30 months; n = 3. Images in upper and lower rows are 100X and 200X magnification, respectively. Scale = 50 μm. Insets are representative images of those shown in Fig. 4C.

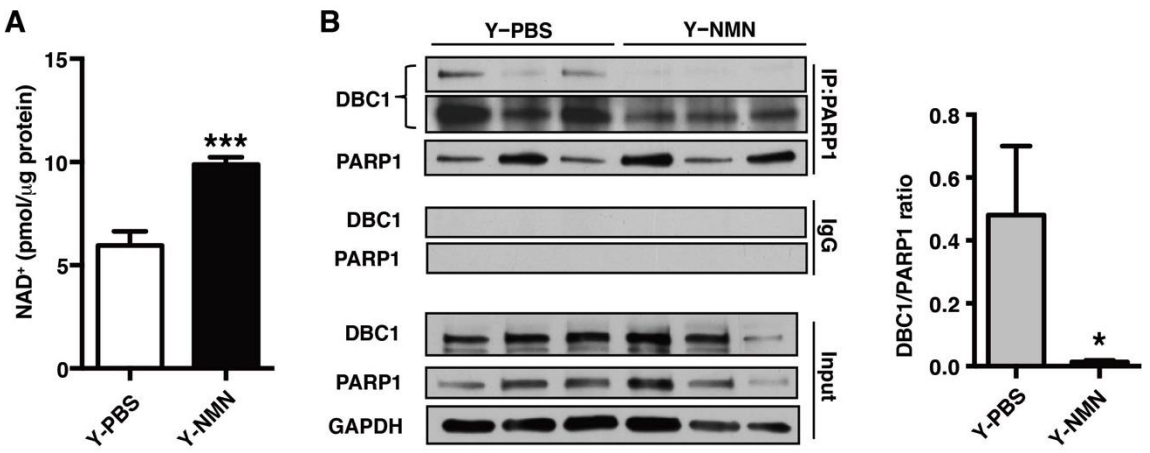

Fig. S15. PARP1-DBC1 interaction in 6-month old mice is reduced by NMN.
Increased relative NAD^+ levels (n=4/group) **(A)** and reduced PARP1-DBC1 interaction **(B)** in the livers of 6-month old mice treated by daily intraperitoneal injections of PBS (Y-PBS) or NMN (Y-NMN) for one week (500 mg/kg/day), mean ± SEM, unpaired two-tailed t-test *p< 0.05, ***p<0.001.

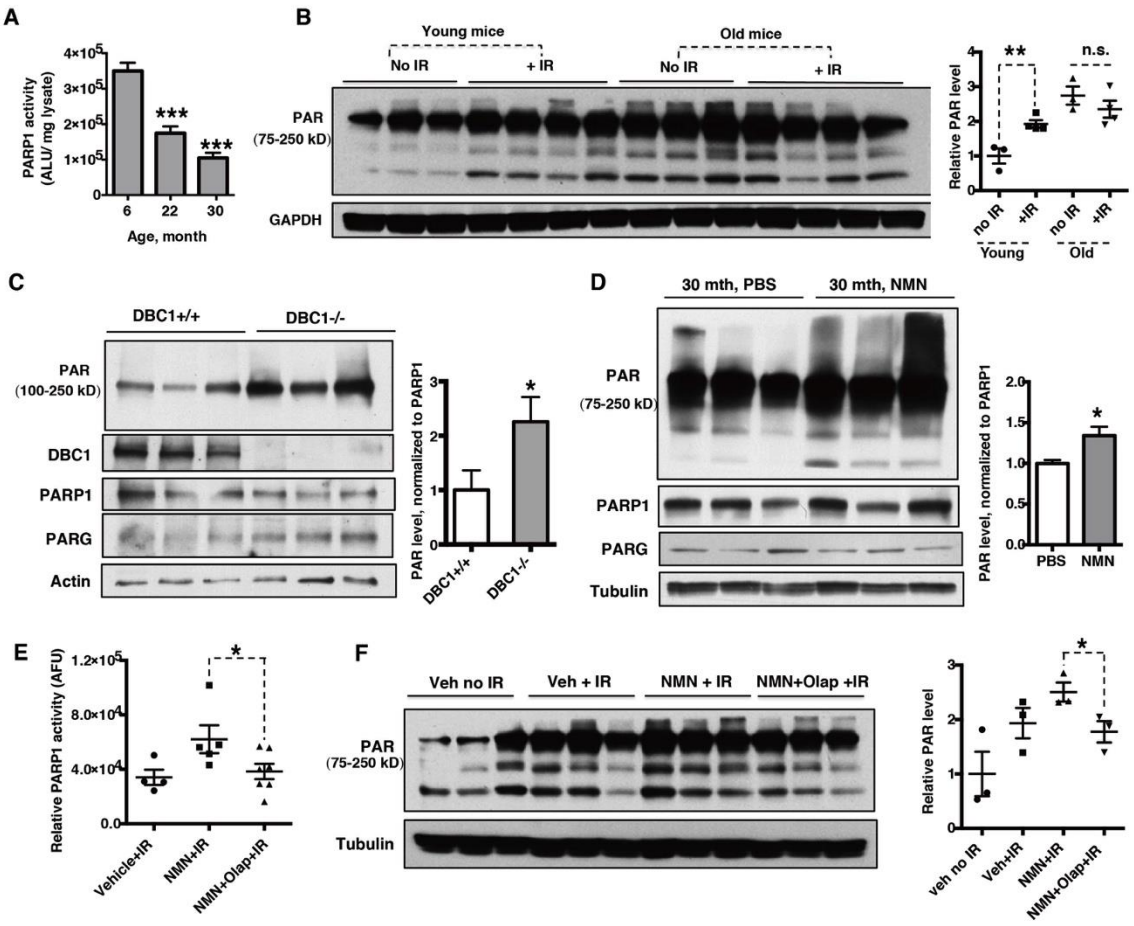

Fig. S16. PARP1 activity decreases with age and is reversed by NMN or genetically ablating DBC1.

(**A**) The enzymatic activity of PARP1 decreases with age. PARP1 was immunoprecipitated from 6-, 22- and 30-month old mouse liver extracts and assayed for maximum activity in the presence of nuclease-treated DNA (n=5 each group, one-way *ANOVA* with Sidak's post-hoc correction). (**B**) PARP1 activation in livers of young and old mice after irradiation**.** Young (10 month) and old (20 month) mice were exposed to a sub-lethal dose of ionizing radiation (+IR, 7.5Gy). PAR levels are quantified on the right. (**C**) PAR levels are higher in DBC1 knockout mice livers than wild-type at 18-20 months of age. Quantification of PAR is shown on the right. (**D**) PAR levels in 30-month old mice livers after NMN treatment as in Fig. 4C. (**E**) and (**F**) The effect of NMN depends on PARP1 activity. The old mice (20 month) were injected intraperitoneally (i.p.) with vehicle (PBS with 10% 2-hydroxypropyl-β-cyclodextrin), NMN (500 mg/kg/d) alone or with the PARP1 inhibitor olaparib (100mg/kg/d) for 7 days. Two hours after the last injection, mice were irradiated with 7.5 Gy and killed 2 hrs later. Equal amounts of liver cell lysates from each group were assayed for PARP1 maximal activity (E) and PAR levels by western blot (F). Errors are SEM, unpaired two-tailed t-test except (A), *p< 0.05, **p< 0.01, ***p<0.001, n.s., not significant.

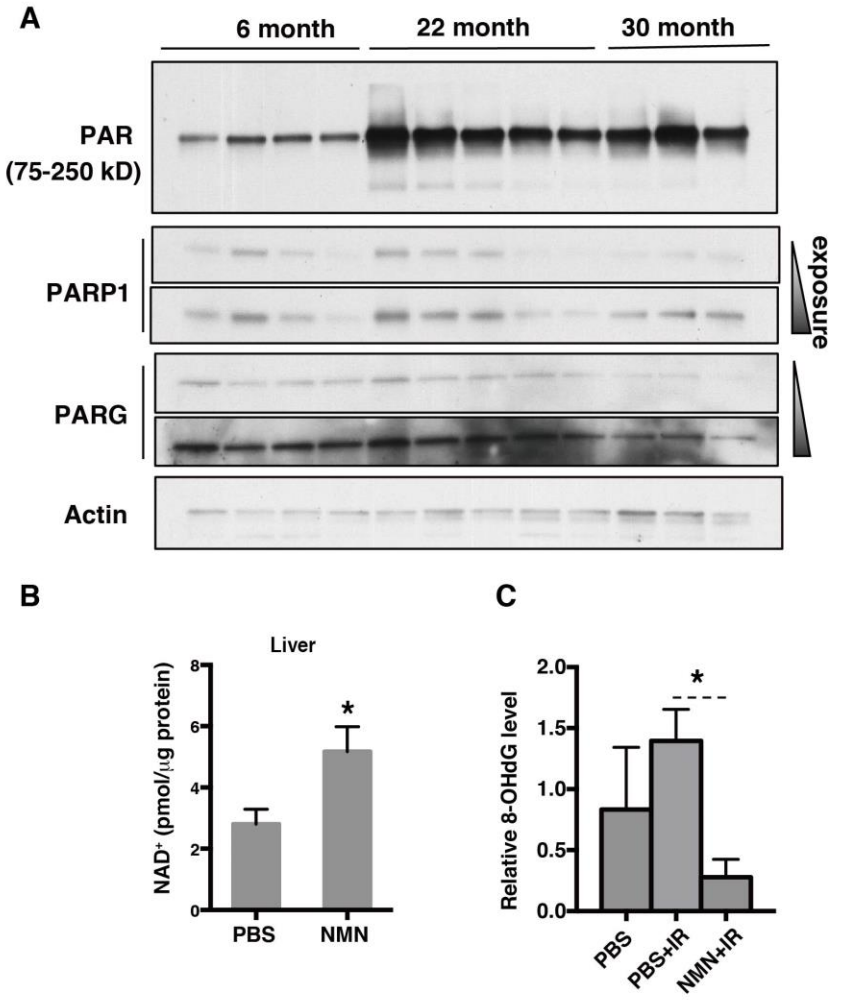

Fig. S17. NMN treatment reduces oxidative DNA damage.
(**A**) PAR levels in 6-, 22- and 30-month old mouse livers. (**B**) NAD^+ levels (n=3 each group) and (**C**) DNA damage marker 8-OHdG (n=3 or 4) in the livers of 26-month old mice after NMN treatment as in Fig. 4C, mean ± SEM, unpaired two-tailed t-test, *p< 0.05.

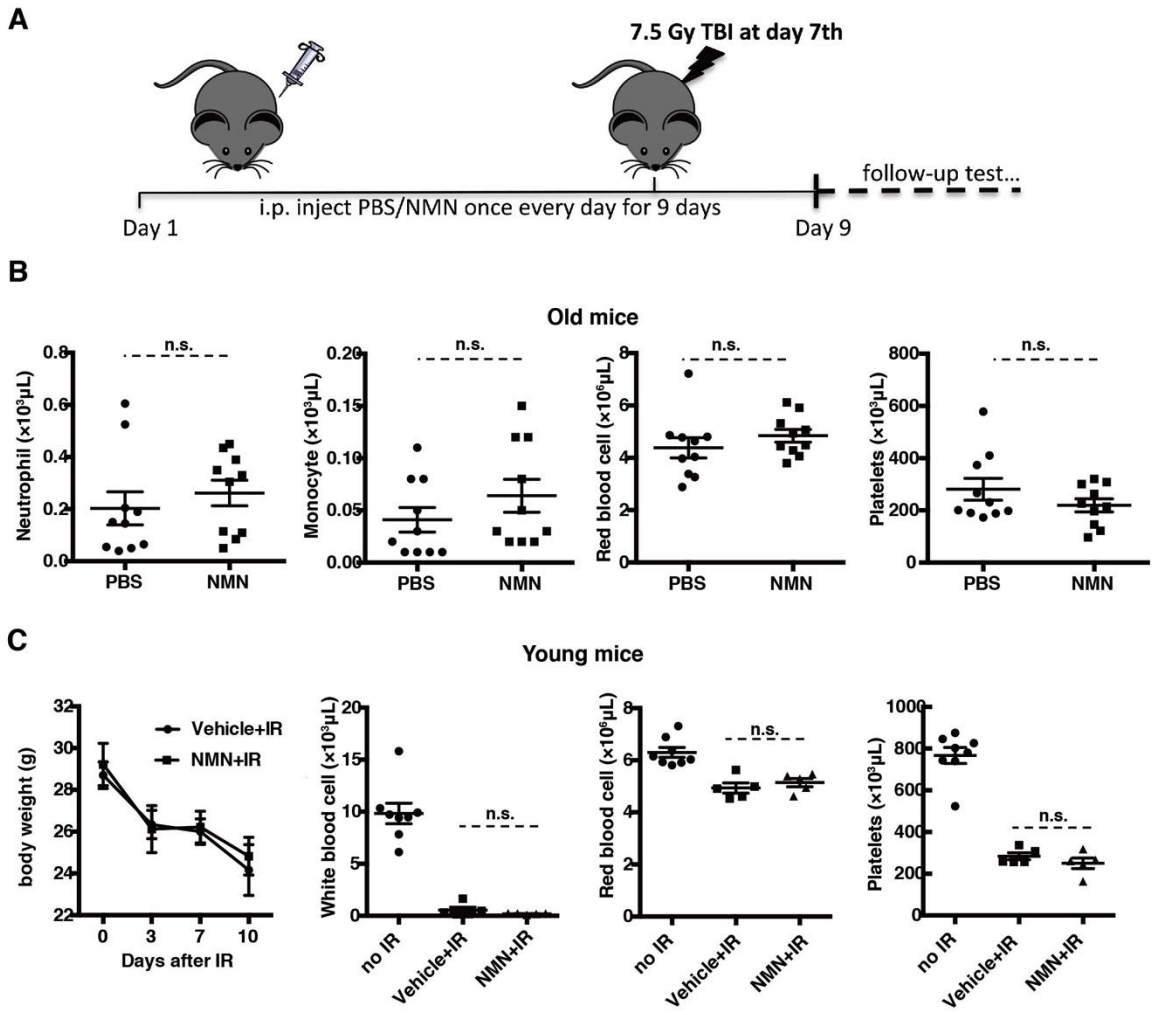

Fig. S18. Additional blood metrics and body weight measurements in mice treated with NMN.

(**A**) Experimental design of experiments in Fig 4I. Two groups of 23-month old mice were pretreated with PBS or NMN (i.p. 500 mg/kg/day) for 7 days then exposed to a single dose of ionizing radiation (7.5 Gy). Mice received injections for 2 more days and blood cell counts were conducted on day 7 and 8 after irradiation. (**B**) Continued from Fig. 4I: Neutrophils, monocyte, red blood cell and platelet counts. (**C**) Continued from Fig.4J: changes in body weight (n=20/group) and white blood cell, red blood cell and platelet counts. Errors are SEM, Mann-Whitney U-test, n.s., not significant.

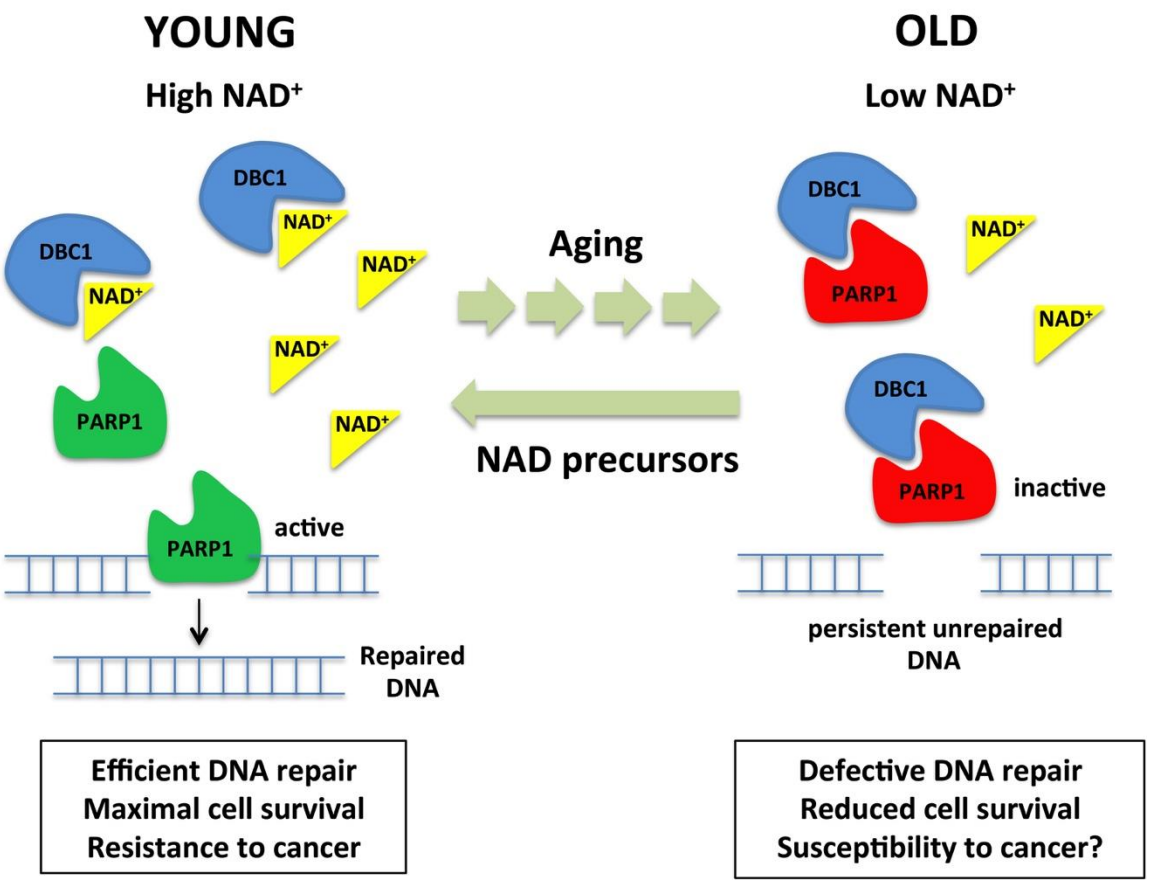

Fig. S19. Model for the regulation of PARP1-DBC1 complex by NAD^+ during aging. Relatively high NAD^+ levels in youth maintain optimal PARP1 activity by limiting the PARP1-DBC1 complex, allowing free PARP1 to facilitate DNA repair and promote cell survival. The regulation of PARP1 by NAD^+ may serve as a negative-feedback loop to limit the consumption of NAD^+ by PARP1 when levels fall below the threshold of cell viability, thereby allowing other modes of DNA repair to take over until NAD^+ levels are restored. As NAD^+ levels decline with aging, PARP1 is increasingly bound to DBC1, resulting in reduced PARP1 and DNA repair activities. Raising NAD^+ levels detaches DBC1 from PARP1 and restores PARP1 and DNA repair activities.

References and Notes

1. R. H. Houtkooper, C. Cantó, R. J. Wanders, J. Auwerx, The secret life of NAD^+: An old metabolite controlling new metabolic signaling pathways. *Endocr. Rev.* **31**, 194–223 (2010). doi:10.1210/er.2009-0026 Medline

2. M. S. Bonkowski, D. A. Sinclair, Slowing ageing by design: The rise of NAD^+ and sirtuin-activating compounds. *Nat. Rev. Mol. Cell Biol.* **17**, 679–690 (2016). doi:10.1038/nrm.2016.93 Medline

3. S. Imai, L. Guarente, NAD^+ and sirtuins in aging and disease. *Trends Cell Biol.* **24**, 464–471 (2014). doi:10.1016/j.tcb.2014.04.002 Medline

4. L. Mouchiroud, R. H. Houtkooper, N. Moullan, E. Katsyuba, D. Ryu, C. Cantó, A. Mottis, Y.-S. Jo, M. Viswanathan, K. Schoonjans, L. Guarente, J. Auwerx, The NAD^+/sirtuin pathway modulates longevity through activation of mitochondrial UPR and FOXO signaling. *Cell* **154**, 430–441 (2013). doi:10.1016/j.cell.2013.06.016 Medline

5. J. Yoshino, K. F. Mills, M. J. Yoon, S. Imai, Nicotinamide mononucleotide, a key NAD^+ intermediate, treats the pathophysiology of diet- and age-induced diabetes in mice. *Cell Metab.* **14**, 528–536 (2011). doi:10.1016/j.cmet.2011.08.014 Medline

6. K. S. Bhullar, B. P. Hubbard, Lifespan and healthspan extension by resveratrol. *Biochim. Biophys. Acta* **1852**, 1209–1218 (2015). doi:10.1016/j.bbadis.2015.01.012 Medline

7. K. Grube, A. Bürkle, Poly(ADP-ribose) polymerase activity in mononuclear leukocytes of 13 mammalian species correlates with species-specific life span. *Proc. Natl. Acad. Sci. U.S.A.* **89**, 11759–11763 (1992). doi:10.1073/pnas.89.24.11759 Medline

8. M. C. Haigis, D. A. Sinclair, Mammalian sirtuins: Biological insights and disease relevance. *Annu. Rev. Pathol.* **5**, 253–295 (2010). doi:10.1146/annurev.pathol.4.110807.092250 Medline

9. V. Anantharaman, L. Aravind, Analysis of DBC1 and its homologs suggests a potential mechanism for regulation of sirtuin domain deacetylases by NAD metabolites. *Cell Cycle* **7**, 1467–1472 (2008). doi:10.4161/cc.7.10.5883 Medline

10. M. Wang, C. J. Herrmann, M. Simonovic, D. Szklarczyk, C. von Mering, Version 4.0 of PaxDb: Protein abundance data, integrated across model organisms, tissues, and cell-lines. *Proteomics* **15**, 3163–3168 (2015). doi:10.1002/pmic.201400441 Medline

11. S. M. Armour, E. J. Bennett, C. R. Braun, X.-Y. Zhang, S. B. McMahon, S. P. Gygi, J. W. Harper, D. A. Sinclair, A high-confidence interaction map identifies SIRT1 as a mediator of acetylation of USP22 and the SAGA coactivator complex. *Mol. Cell. Biol.* **33**, 1487–1502 (2013). doi:10.1128/MCB.00971-12 Medline

12. A. S. Mildvan, Z. Xia, H. F. Azurmendi, V. Saraswat, P. M. Legler, M. A. Massiah, S. B. Gabelli, M. A. Bianchet, L.-W. Kang, L. M. Amzel, Structures and mechanisms of Nudix hydrolases. *Arch. Biochem. Biophys.* **433**, 129–143 (2005). doi:10.1016/j.abb.2004.08.017 Medline

13. J. P. Gagné, M. Isabelle, K. S. Lo, S. Bourassa, M. J. Hendzel, V. L. Dawson, T. M. Dawson, G. G. Poirier, Proteome-wide identification of poly(ADP-ribose) binding proteins and poly(ADP-ribose)-associated protein complexes. *Nucleic Acids Res.* **36**, 6959–6976 (2008). doi:10.1093/nar/gkn771 Medline

14. J. E. Kim, J. Chen, Z. Lou, DBC1 is a negative regulator of SIRT1. *Nature* **451**, 583–586 (2008). doi:10.1038/nature06500 Medline

15. H. Yang, T. Yang, J. A. Baur, E. Perez, T. Matsui, J. J. Carmona, D. W. Lamming, N. C. Souza-Pinto, V. A. Bohr, A. Rosenzweig, R. de Cabo, A. A. Sauve, D. A. Sinclair, Nutrient-sensitive mitochondrial NAD^+ levels dictate cell survival. *Cell* **130**, 1095–1107 (2007). doi:10.1016/j.cell.2007.07.035 Medline

16. M. Hasmann, I. Schemainda, FK866, a highly specific noncompetitive inhibitor of nicotinamide phosphoribosyltransferase, represents a novel mechanism for induction of tumor cell apoptosis. *Cancer Res.* **63**, 7436–7442 (2003). Medline

17. F. Berger, C. Lau, M. Dahlmann, M. Ziegler, Subcellular compartmentation and differential catalytic properties of the three human nicotinamide mononucleotide adenylyltransferase isoforms. *J. Biol. Chem.* **280**, 36334–36341 (2005). doi:10.1074/jbc.M508660200 Medline

18. P. Bork, K. Hofmann, P. Bucher, A. F. Neuwald, S. F. Altschul, E. V. Koonin, A superfamily of conserved domains in DNA damage-responsive cell cycle checkpoint proteins. *FASEB J.* **11**, 68–76 (1997). Medline

19. T. Zhang, J. G. Berrocal, J. Yao, M. E. DuMond, R. Krishnakumar, D. D. Ruhl, K. W. Ryu, M. J. Gamble, W. L. Kraus, Regulation of poly(ADP-ribose) polymerase-1-dependent gene expression through promoter-directed recruitment of a nuclear NAD^+ synthase. *J. Biol. Chem.* **287**, 12405–12416 (2012). doi:10.1074/jbc.M111.304469 Medline

20. R. Krishnakumar, W. L. Kraus, PARP-1 regulates chromatin structure and transcription through a KDM5B-dependent pathway. *Mol. Cell* **39**, 736–749 (2010). doi:10.1016/j.molcel.2010.08.014 Medline

21. V. Gorbunova, A. Seluanov, Z. Mao, C. Hine, Changes in DNA repair during aging. *Nucleic Acids Res.* **35**, 7466–7474 (2007). doi:10.1093/nar/gkm756 Medline

22. M. Hamaguchi, J. L. Meth, C. von Klitzing, W. Wei, D. Esposito, L. Rodgers, T. Walsh, P. Welcsh, M.-C. King, M. H. Wigler, DBC2, a candidate for a tumor suppressor gene involved in breast cancer. *Proc. Natl. Acad. Sci. U.S.A.* **99**, 13647–13652 (2002). doi:10.1073/pnas.212516099 Medline

23. M. W. Audeh, J. Carmichael, R. T. Penson, M. Friedlander, B. Powell, K. M. Bell-McGuinn, C. Scott, J. N. Weitzel, A. Oaknin, N. Loman, K. Lu, R. K. Schmutzler, U. Matulonis, M. Wickens, A. Tutt, Oral poly(ADP-ribose) polymerase inhibitor olaparib in patients with *BRCA1* or *BRCA2* mutations and recurrent ovarian cancer: A proof-of-concept trial. *Lancet* **376**, 245–251 (2010). doi:10.1016/S0140-6736(10)60893-8 Medline

24. D. B. Lombard, K. F. Chua, R. Mostoslavsky, S. Franco, M. Gostissa, F. W. Alt, DNA repair, genome stability, and aging. *Cell* **120**, 497–512 (2005). doi:10.1016/j.cell.2005.01.028 Medline

25. B. P. Hubbard, A. P. Gomes, H. Dai, J. Li, A. W. Case, T. Considine, T. V. Riera, J. E. Lee, S. Y. e, D. W. Lamming, B. L. Pentelute, E. R. Schuman, L. A. Stevens, A. J. Y. Ling, S. M. Armour, S. Michan, H. Zhao, Y. Jiang, S. M. Sweitzer, C. A. Blum, J. S. Disch, P. Y. Ng, K. T. Howitz, A. P. Rolo, Y. Hamuro, J. Moss, R. B. Perni, J. L. Ellis, G. P. Vlasuk, D. A. Sinclair, Evidence for a common mechanism of SIRT1 regulation by allosteric activators. *Science* **339**, 1216–1219 (2013). doi:10.1126/science.1231097 Medline

26. J. R. Revollo, A. A. Grimm, S. Imai, The NAD biosynthesis pathway mediated by nicotinamide phosphoribosyltransferase regulates Sir2 activity in mammalian cells. *J. Biol. Chem.* **279**, 50754–50763 (2004). doi:10.1074/jbc.M408388200 Medline

27. P. A. Loeffler, M. J. Cuneo, G. A. Mueller, E. F. DeRose, S. A. Gabel, R. E. London, Structural studies of the PARP-1 BRCT domain. *BMC Struct. Biol.* **11**, 37 (2011).

28. D. A. Wacker, D. D. Ruhl, E. H. Balagamwala, K. M. Hope, T. Zhang, W. L. Kraus, The DNA binding and catalytic domains of poly(ADP-ribose) polymerase 1 cooperate in the regulation of chromatin structure and transcription. *Mol. Cell. Biol.* **27**, 7475–7485 (2007). doi:10.1128/MCB.01314-07 Medline

29. A. P. Gomes, N. L. Price, A. J. Y. Ling, J. J. Moslehi, M. K. Montgomery, L. Rajman, J. P. White, J. S. Teodoro, C. D. Wrann, B. P. Hubbard, E. M. Mercken, C. M. Palmeira, R. de Cabo, A. P. Rolo, N. Turner, E. L. Bell, D. A. Sinclair, Declining NAD^+ induces a pseudohypoxic state disrupting nuclear-mitochondrial communication during aging. *Cell* **155**, 1624–1638 (2013). doi:10.1016/j.cell.2013.11.037 Medline

30. S. F. Altschul, T. L. Madden, A. A. Schäffer, J. Zhang, Z. Zhang, W. Miller, D. J. Lipman, Gapped BLAST and PSI-BLAST: A new generation of protein database search programs. *Nucleic Acids Res.* **25**, 3389–3402 (1997). doi:10.1093/nar/25.17.3389 Medline

31. T. Lassmann, E. L. Sonnhammer, Kalign—An accurate and fast multiple sequence alignment algorithm. *BMC Bioinformatics* **6**, 298 (2005). doi:10.1186/1471-2105-6-298 Medline

32. J. Pei, N. V. Grishin, PROMALS: Towards accurate multiple sequence alignments of distantly related proteins. *Bioinformatics* **23**, 802–808 (2007). doi:10.1093/bioinformatics/btm017 Medline

33. J. Söding, A. Biegert, A. N. Lupas, The HHpred interactive server for protein homology detection and structure prediction. *Nucleic Acids Res.* **33** (suppl. 2), W244–W248 (2005). doi:10.1093/nar/gki408 Medline

34. J. A. Cuff, M. E. Clamp, A. S. Siddiqui, M. Finlay, G. J. Barton, JPred: A consensus secondary structure prediction server. *Bioinformatics* **14**, 892–893 (1998). doi:10.1093/bioinformatics/14.10.892 Medline

35. A. Šali, T. L. Blundell, Comparative protein modelling by satisfaction of spatial restraints. *J. Mol. Biol.* **234**, 779–815 (1993). doi:10.1006/jmbi.1993.1626 Medline

36. D. Cozzetto, A. Tramontano, Relationship between multiple sequence alignments and quality of protein comparative models. *Proteins* **58**, 151–157 (2005). doi:10.1002/prot.20284 Medline

37. J. P. Rodrigues, M. Levitt, G. Chopra, KoBaMIN: A knowledge-based minimization web server for protein structure refinement. *Nucleic Acids Res.* **40** W323–W328 (2012). doi:10.1093/nar/gks376 Medline

38. Z. Mao, Y. Jiang, X. Liu, A. Seluanov, V. Gorbunova, DNA repair by homologous recombination, but not by nonhomologous end joining, is elevated in breast cancer cells. *Neoplasia* **11**, 683–691 (2009). doi:10.1593/neo.09312 Medline

39. Z. Mao, C. Hine, X. Tian, M. Van Meter, M. Au, A. Vaidya, A. Seluanov, V. Gorbunova, SIRT6 promotes DNA repair under stress by activating PARP1. *Science* **332**, 1443–1446 (2011). doi:10.1126/science.1202723 Medline

40. F. Rosenthal, K. L. H. Feijs, E. Frugier, M. Bonalli, A. H. Forst, R. Imhof, H. C. Winkler, D. Fischer, A. Caflisch, P. O. Hassa, B. Lüscher, M. O. Hottiger, Macrodomain-containing proteins are new mono-ADP-ribosylhydrolases. *Nat. Struct. Mol. Biol.* **20**, 502–507 (2013). doi:10.1038/nsmb.2521 Medline